RSC Advances

RSC Publishing

PAPER

View Article Online
View Journal | View Issue

Cite this: *RSC Advances*, 2013, **3**, 17120

Graphene-loaded sodium alginate nanocomposite membranes with enhanced isopropanol dehydration performance *via* a pervaporation technique

Dharupaneedi P. Suhas,[a] Anjanapura V. Raghu,*[a] Han M. Jeong[b] and Tejraj M. Aminabhavi[a]

Received 26th April 2013,
Accepted 9th July 2013

DOI: 10.1039/c3ra42062k

www.rsc.org/advances

Graphene-loaded sodium alginate (NaAlg) nanocomposite membranes have been prepared to enhance the pervaporation (PV) dehydration of isopropanol. The effect of graphene loading on the physico-chemical properties, micro-morphology and barrier performance of the derived nanocomposite membranes was investigated as a function of temperature and feed water composition of the isopropanol mixture. The interaction of graphene with the NaAlg matrix as well as water and isopropanol seems to influence the thermal, kinetic and Arrhenius activation energy parameters. At the lowest concentration of graphene, the membrane performance was optimum with a permeance value of 3122 GPU and a selectivity of 4623 for a 10 wt.% water containing feed mixture at 30 °C. Flory–Huggins theory could explain the polymer–solvent interaction as well as equilibrium swelling; both of these affected the membrane performance.

Introduction

Conventionally, even though distillation is the most versatile method to separate liquid–liquid mixtures, the method is not economic for extracting high purity solvents from azeotropic mixtures. Azeotropic distillation, on the other hand, requires an entrainer, which is not recommended for separation, since it causes environmental pollution problems.[1–3] Pervaporation (PV), on the other hand, is considered to be a potential separation method, since it deals with minor components (usually <10 wt.%) of the liquid mixture and consumes only a small part of the latent heat of energy. The success of PV separation is largely due to the development of selective membranes that are the heart of the process.[4] Innumerable attempts have been made in the literature to develop different types of membranes, particularly for the separation of water–isopropanol mixtures as pure isopropanol is required in the pharmaceutical and electronics industries.[5]

Despite the superior performance of inorganic membranes (*viz.*, zeolites and ceramics),[6,7] the high cost involved in their processing limits their commercial application. On the other hand, organic polymeric materials have proved to be the most suitable and versatile barrier membranes due to their good film forming ability, low-cost and ease of physico-chemical modification.[8] Hydrophilic polymers are particularly appropriate as membrane materials to dehydrate isopropanol as these have high water sorption abilities as well as enhanced chemical and thermal stability in aggressive solvent media. Among the many organic polymers, sodium alginate (NaAlg), a naturally occurring hydrophilic biopolymer, has been widely used as a membrane in PV separation,[9] even though its main drawback is high swelling, which sacrifices the selectivity and mechanical strength properties, which is not a favorable situation in PV separation. Over the past decade, continuous efforts have been made by our own laboratory, as well as others, to develop novel types of membranes, which include cross-linking, grafting, blending and composite membranes.[10–15] Such membranes are typically formed through an intimate and homogeneous dispersion of filler particles in the polymer matrix,[16] and these have proved to affect the membrane performance to a considerable extent. The surface chemistry of filler particles, chemical structure, particle size distribution and aspect ratio are some of the major factors which control the barrier properties of such membranes.[17,18]

In recent years, the use of graphene oxide (GO) as a filler has attracted much interest, since it is known to produce a dramatic improvement in the mechanical and barrier properties of the derived membrane even if present at very low concentrations.[19] The GO sheets derived from graphene nanosheets are *quasi*-two-dimensional honeycomb lattice type structures with oxygen containing functional groups on their basal planes and edges, such as hydroxyl, epoxide, carbonyl and carboxylic acid.[20] These functional groups can be effective in improving the interfacial bonding between GO sheets and the polymer matrix, thereby achieving a uniform dispersion

[a]*Materials Science Division, Poornaprajna Institute of Scientific Research, Bengaluru 562110, India. E-mail: gsraghu2003@yahoo.co.in; raghu@poornaprajna.org*
[b]*Department of Chemistry, University of Ulsan, Ulsan, Republic of Korea-680 749*

when embedded in the polymer matrix.[21] These properties prompted us to utilize GO as a filler material in the NaAlg matrix to develop nanocomposite membranes used in the PV dehydration of isopropanol (IPA).[22] Furthermore, owing to the high aspect ratio of GO sheets and their distinctive two-dimensional structure, they have been used as filler materials to improve the barrier/separation performances.[23,24]

Even though overcoming a trade-off in selectivity and permeance during the PV separation of a water–organic mixture is a formidable task, several membranes have partially achieved this goal. In this investigation, highly oxygenated surface functionalized graphene sheets (FGSs), due to their water selective intercalation structure, are an interesting candidate for incorporation into the NaAlg matrix to boost the PV dehydration of IPA. The formation of well-defined FGS–NaAlg nanocomposite membranes is assessed by the use of analytical techniques such as Fourier transform infrared spectroscopy (FTIR), X-ray diffraction (XRD), field emission scanning electron microscopy (FE-SEM), thermogravimetry (TGA) and contact angle (CA) measurements. The test of the membrane performance for PV separation of water–IPA mixtures as a function of temperature, feed mixture composition and filler loading indicated the effectiveness of the nanocomposite membrane compared to the nascent NaAlg membrane. Several process parameters *viz.*, sorption (thermodynamic), diffusion (kinetic) and Arrhenius activation energy (energy barrier for permeation and diffusion) parameters have been assessed to understand the superior PV results achieved by using the nanocomposite membranes. The results of this study are explained in terms of the Flory–Huggins interaction parameters as well as the extent of equilibrium swelling.

Experimental

Materials

Natural graphite (HC-908) was purchased from Hyundai Coma Co. Ltd., South Korea. Sodium alginate, isopropanol, methanol, hydrochloric acid, nitric acid, potassium chloride and glutaraldehyde (GA) were all purchased from s. d. Fine Chemicals, Mumbai, India. Absolute ethanol (EtOH) (99.9%) was purchased from Commercial Alcohols, Brampton, Canada. All the other chemicals used were of reagent grade and were used without purification. Double distilled water was used throughout the experimental study.

Preparation of FGSs

FGSs were prepared from graphite using the Brondie method.[25] A round bottom flask with 200 mL of fuming nitric acid was cooled to 0 °C to which 10 g of graphite powder was added under constant stirring. The temperature of the reaction flask was gradually increased to an ambient temperature along with the addition of potassium chloride. This mixture was stirred magnetically overnight and transferred to a beaker containing 3 L of double distilled water. The obtained graphite oxide was filtered, washed with distilled water several times until it turned neutral and dried in a vacuum oven at 100 °C. Elemental analysis showed that graphite oxide has the empirical elemental structure: $C_{10}O_{3.45}H_{1.58}$.

To obtain FGSs, dried graphite oxide was charged in a quartz tube under a constant flow of nitrogen gas for 5 min. The quartz tube was quickly introduced to a furnace at 1100 °C for 1 min to split the graphite oxide into individual nano graphene sheets by releasing CO_2.[26] Elemental analysis of the FGSs showed its empirical elemental structure to be: $C_{10}O_{0.78}H_{0.38}$. The surface of the FGSs as measured by Brunauer, Emmett and Teller measurement using a nitrogen adsorption technique in the dry state was 428 $m^2\ g^{-1}$. Knowing that a single layer of the FGSs has a surface area of 2600 $m^2\ g^{-1}$, the recorded surface area measurement suggested multi-layer FGSs containing six layers.

Membrane fabrication. The method used to prepare FGS-loaded NaAlg nanocomposite membranes with a uniform dispersion of FGS nanoparticles was based on solution-casting and solvent evaporation.[27] In a typical procedure, 4 g of NaAlg was dissolved in 100 mL of water. In a separate flask, the required amount of FGSs was stirred with 30 mL of water for 3 h and sonicated for 2 h, to which 10 wt.% of NaAlg solution was added and stirred for 12 h. The remaining NaAlg solution was added along with a drop-wise addition of 1.5 mL of 1 N sodium hydroxide solution to decrease the viscosity of the solution to achieve homogeneous mixing. Both the solutions were then mixed for 24 h and kept overnight to release any gases. The resulting solution was poured onto a perfectly aligned flat clean glass plate dried under ambient conditions; the dried membrane was peeled off from the glass plate and immersed in a cross-linking solution bath containing a water–acetone mixture (30 : 70) along with 2 mL of glutaraldehyde and 1 mL of hydrochloric acid for 6 h. The cross-linked membranes were removed from the bath and washed repeatedly with methanol solution. Using the above procedure, 1, 2 and 3 wt.% FGS-loaded NaAlg nanocomposite membranes were prepared and are designated as: NaAlg-1, NaAlg-2 and NaAlg-3, respectively. The nascent NaAlg was prepared in the same manner without the addition of FGSs.

Membrane characterization. To understand the chemical interaction between the FGSs and NaAlg, FTIR spectra of the pure FGSs, nascent NaAlg and FGS-loaded NaAlg nanocomposite membranes were scanned in the range of 400–4000 cm^{-1} using a Bruker Alpha-T Spectrometer by the KBr method (32 scans and with a resolution of 4 cm^{-1}) for each spectrum.

A Bruker D-2 phaser X-ray diffractometer was used to study the solid state morphology of the membranes in powder form. X-rays of 1.5406 Å wavelength were obtained by a Ni filtered Cu-Kα radiation source and the sample was scanned in the range of 2θ = 5–60° at a scanning rate of 2° min^{-1}.

The morphology and thickness of nanocomposite membranes was examined by field emission scanning electron microscopy (FE-SEM) using a FE-SEM Zeiss Ultra 55 instrument and by creating a conductive layer of sputtered gold.

Thermal degradation of the nascent NaAlg and FGS-loaded nanocomposite membranes were investigated by a thermal gravimetric analyzer (TGA Q500; courtesy of Dr K. V. S. N. Raju, IICT, Hyderabad) under a nitrogen atmosphere with a flow capacity of 50 mL min^{-1}. The scan was carried out from 40 to

600 °C at a heating rate of 10 °C min^{-1}. For each analysis, about 6–9 mg of the sample was taken in aluminum pans.

To investigate the surface properties of the membrane, static contact angle measurements were performed according to the sessile drop method using a Data Physics OCA-20 at 25 °C. Membranes were dried perfectly in a vacuum desiccator prior to the contact angle measurements. A piece of the membrane (1 cm × 7 cm) was adhered to a clean and smooth glass slide on which a 2 μL deionized water droplet was placed and the droplet image was captured using a microscope coupled with a CCD camera (courtesy of Prof. S. K. Biswas, IISc, Bangalore). To reduce the evaporation losses, measurements were done within 10 s. All the reported values are the averages of eight measurements taken at different locations on the same membrane surface.

Equilibrium swelling. Equilibrium swelling experiments were performed gravimetrically at 30 °C for the IPA–water mixture with a variable water composition of 10, 20, 30 and 40 wt.%. The initial weight of the circularly cut (diameter = 2.5 cm) NaAlg and FGS-incorporated NaAlg nanocomposite membranes were taken on a single pan digital microbalance, Sartorius BSA224, having a sensitivity of ±0.001 mg. Samples were placed inside specially designed air tight test bottles containing 30 cm^3 of the test solvent and were kept in a hot air oven maintained at 30 °C. Dry nanocomposite membranes were equilibrated by soaking in respective different compositions of the feed mixtures in sealed test bottles maintained at 30 °C for 48 h. The weight of the samples was taken after removal from the bottle (to check for degree of swelling of each membrane) and the surface adhered liquid droplets were removed by gently pressing them between filter paper wraps. In order to minimize solvent evaporation losses, this step was completed within, approximately 15–20 s. Later, the membranes were completely dried and their weights remained almost the same as the initial weight with a small difference of only ± 0.5%. The equilibrium swelling (E.S.) (%) was then calculated using:

$$\text{E.S. (\%)} = \left(\frac{W_s - W_d}{W_d}\right) \times 100 \quad (1)$$

where W_s is the weight of the membrane after swelling and W_d is the weight of the dry membrane before swelling.

Pervaporation experiments. PV experiments were carried out using an indigenously designed stainless steel unit described elsewhere[28] consisting of two components *viz.*, feed tank and permeate cell. The membrane with an effective area of 3.84 × 10^{-3} m^2 was placed tightly using two O-shaped Teflon rings supported on a porous stainless steel support. The feed tank was a double-walled cell with a feed capacity of 500 mL. With the outer jacket connected to thermostatic bath (Grant, UK, model GD-120), the temperature in the feed tank was maintained by pumping water at the desired temperature that was circulated into the outer jacket of the feed tank. Further, the feed tank was provided with a thermometer to monitor the feed temperature and a stirrer rotating at 50 rpm to mix the liquid mixture uniformly.

The feed mixture was maintained at atmospheric pressure and the permeate was maintained at <5 mbar pressure with the help of a double-stage vacuum pump. The feed mixture of different compositions and at different temperatures was first equilibrated for 2 h before collecting the permeate sample. After 2 h of batch operation, a constant flux was obtained and thereafter, permeate samples were collected by a cold trap immersed in a liquid nitrogen container. The samples were weighed on a Sartorius BSA224 balance. The feed mixture composition was analyzed by measuring the refractive index with the help of a refractometer (Mettler, Toledo) to an accuracy of ±0.0001 units. To calculate this, a previously established standard graph of refractive index *vs.* known mixture composition was used at 30 ± 0.1 °C. The composition of permeate was also determined by gas chromatography (Trace 700, Thermo-Fischer) equipped with a TCD detector and a Parapak-Q packed column. The same disc was re-used for subsequent analysis at increasing water content of the feed and at increasing temperature. However, the feed mixture was maintained at a constant composition by compensating for any loss of water. At least three different readings were taken independently and the average values were considered.

In this paper, pervaporation data are reported in driving force normalized form *viz.*, permeance (P_i/l) and selectivities (α_{ij}) as proposed by Wijmans[29] as it is the most appropriate way to report the PV data, since it gives the exact idea about the intrinsic properties of the membrane. Thus, permeance was calculated as:

$$\frac{P_i}{l} = \frac{D_i K_i}{l} = \frac{j_i}{\left(p_i^f - p_i^p\right)} \quad (2)$$

where P_i is permeability of the component i, where i represents water or IPA molecules; D_i and K_i represent the diffusion and sorption coefficients of the component i, respectively, l is the membrane thickness; p_i^f and p_i^p are the vapour pressure of the component i in the feed and the permeate, respectively; j_i is the molar flux of the component i, which was calculated as:

$$j_i = \frac{J_i v_i}{m_i} \quad (3)$$

Here, J_i is the flux (g m^{-2} h^{-1}), m_i is the molecular weight (g mol^{-1}) and v_i is the molar volume (22.4l (STP) mol^{-1}) of the component i.

The relationship between partial vapor pressure (p_i^f), molar concentration (x_i) and activity coefficient (γ_i) of the individual components were established through the van Laar relationship[30] as:

$$p_i^f = x_i \gamma_i p_i^s \quad (4)$$

The saturated vapor pressure (p_i^s) of the component i of the mixture was calculated using the Antoine equation:[31]

$$\log p_i^s = \frac{A - B}{T + C} \quad (5)$$

where A, B and C are the Antoine constants taken from the literature[32] and T is the temperature in degrees Kelvin. In order to calculate membrane selectivity (α_{ij}), we have used the

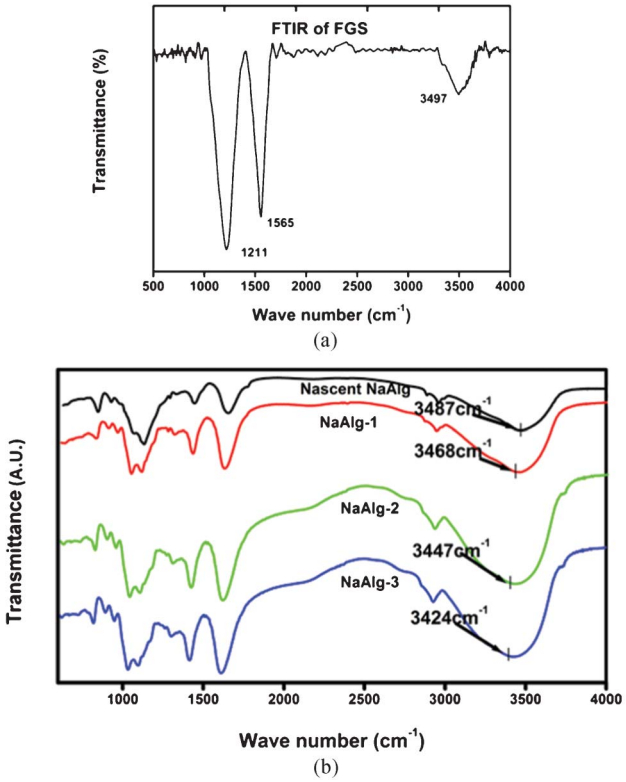

Fig. 1 (a) FTIR spectrum of the FGSs showing the presence of oxygenated functional groups. (b) FTIR spectra of the nascent and NaAlg with various FGS concentrations, showing an increase in red shift with increase in FGS loading.

protocol proposed by Baker *et al.*,[33] according to which, for a binary mixture, selectivity is the ratio of permeabilites or permeances of the components i and j through the membrane which was calculated as:

$$\alpha_{ij} = \frac{P_i/l}{P_j/l} \quad (6)$$

Results and discussion

Characterization of membranes

FTIR. The FTIR spectrum of the FGSs (Fig. 1(a)) shows broad absorption bands at 3430, 1540 and 1230 cm^{-1} that are attributed to –OH, C=C and C–O bond vibrations, respectively.[34] In the case of the nanocomposite membranes as shown in Fig. 1(b), the two prominent peaks observed at 1620 and 1076 cm^{-1} represent the symmetric C=O and asymmetric O–C–O stretching of the carboxyl group, respectively, while the characteristic free –OH stretching vibrations are seen between 3400 and 3500 cm^{-1}. Notably, there is a slight red-shift of the –OH absorption with increasing concentration of the FGSs, which suggests an enhanced hydrogen-bonding interaction between the NaAlg and the FGSs. Due to the very fine dispersion of the FGS particles in the NaAlg matrix; the peak

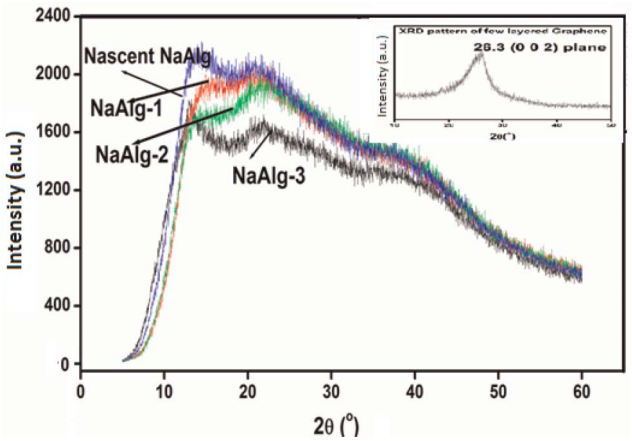

Fig. 2 Powder XRD pattern of nascent and FGS loaded NaAlg showing decrease in intensity with increase in FGS loading (inset: XRD of the raw FGSs).

intensity of the FGS absorption is either very low or not observed. Also, there is an increase in the intensity of the –OH absorbance peak with increased FGS concentration, mainly due to the enhanced polar nature of the membrane. The present results are in good agreement with those reported by Magalad *et al.*[35]

X-Ray diffractogram. XRD diffractograms of all the membranes, along with the FGSs (inset), presented in Fig. 2, show a diffraction peak at a θ of 26.3° for the FGSs, which corresponds to the (0 0 2) plane; a similar observation was made by Choi *et al.*[36] However, for the nascent NaAlg, two characteristic peaks are observed at 15.89° and 28.62° that are in agreement with the reported data.[37] With increasing FGS loading, the peak intensity has diminished and disappeared at 3 wt.% concentration of FGSs due to an increased interaction between the oxygenated functional groups of the FGSs and the polar functional groups of NaAlg. However, the peak corresponding to the FGSs did not appear in the nanocomposite membrane, indicating its uniform dispersion in the NaAlg matrix.

Field emission scanning electron microscopy (FE-SEM). The FE-SEM image of the nascent NaAlg has no bright spots due to its non-conductive nature (see Fig. 3(a)), but the FGS-loaded nanocomposite shows bright spots with some wrinkles and folding on the surface[38] (Fig. 3(b)). Fig. 3(c) and 3(d) show FE-SEM images of NaAlg-1 and NaAlg-3, respectively in which the FGS particles are highlighted by orange colored arrows, and which reveal the smooth surface morphology due to the nano-scale agglomerated distribution of FGS particles. Similar trends were reported earlier by Han *et al.*,[39] in the case of chitosan–graphene nanocomposites. This type of morphology facilitates the formation of nano-voids between the interface of the FGSs and the NaAlg, which would result in the selective permeation of water molecules from the IPA–water mixtures. The size of the agglomerates increases with increasing FGS loading up to 2 wt.%, beyond which the extent of agglomeration reaches the ''saturation limit'', resulting in a decrease of membrane performance.

Thermogravimetric analysis (TGA). The TGA curves for the non-oxidative degradation (due to the presence of a nitrogen

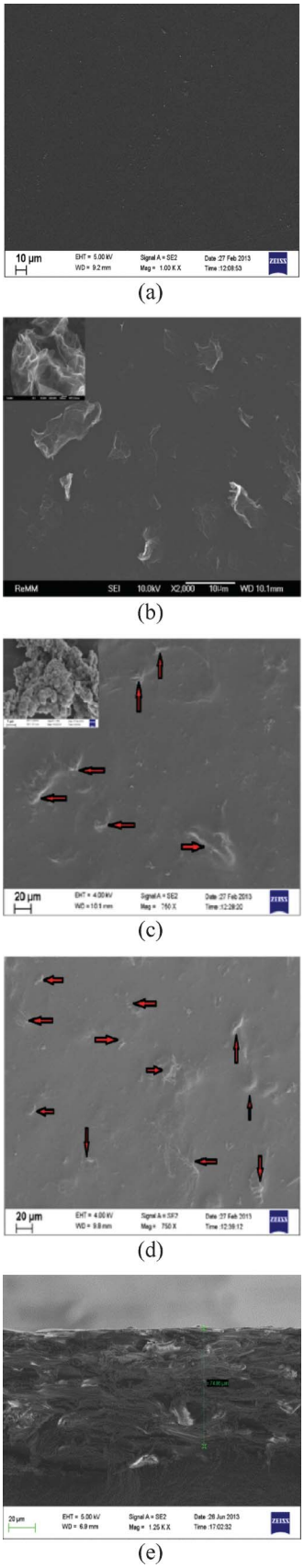

Fig. 3 FE-SEM images of (a) nascent NaAlg, (b) the FGSs, (c) NaAlg-1 (inset: showing nano-agglomeration) and (d) NaAlg-3 showing dispersion of FGS particles in the membrane matrix. (e) Cross-section of NaAlg-3 showing a cross section length of 74 μm.

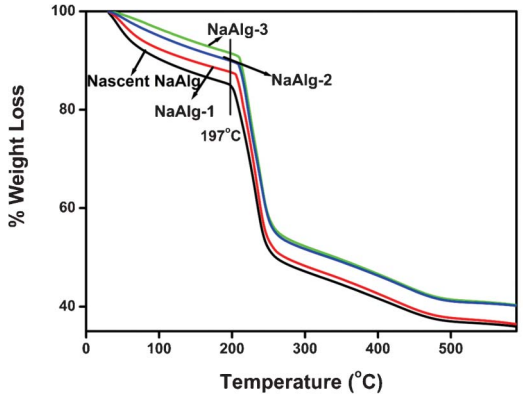

Fig. 4 TGA curves of the nascent NaAlg, NaAlg-1, NaAlg-2 and NaAlg-3 membranes showing an increase in degradation temperature as the FGS concentration increases in the NaAlg matrix.

atmosphere) of the membranes displayed in Fig. 4 show a major weight loss of 40 wt.% at about 200 °C due to the thermal degradation of NaAlg. However, at increasing concentrations of the FGSs, a decrease in weight % loss and an increase in the degradation temperature occurred. The oxygenated functional groups of the FGSs might interact with the polar groups of the NaAlg, thus forming a well defined interface, which restricts the thermal motion of the NaAlg chains. At higher concentrations of the FGSs, high thermal stability is prevalent.[40]

Contact angle studies. Water contact angle is typically used as an indicator of hydrophilicity of the membrane. The smaller the contact angle, the higher the hydrophilicity and *vice versa*. The effect of FGS loading on the hydrophilicity of the membrane as presented in Fig. 5 suggests an increase in hydrophilicity of the NaAlg membrane at a higher concentration of FGS nanoparticles. This is due to the presence of the oxygenated functional groups of the FGSs, making the membranes more hydrophilic. Ganesh *et al.*[41] reported similar

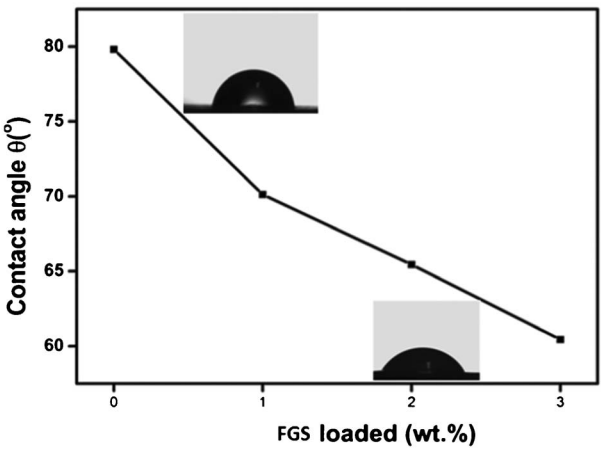

Fig. 5 Change in water contact angle (°) of FGS–NaAlg nanocomposites as a function of FGS loading in wt.%, showing an increase in hydrophilicity with increase in FGS loading.

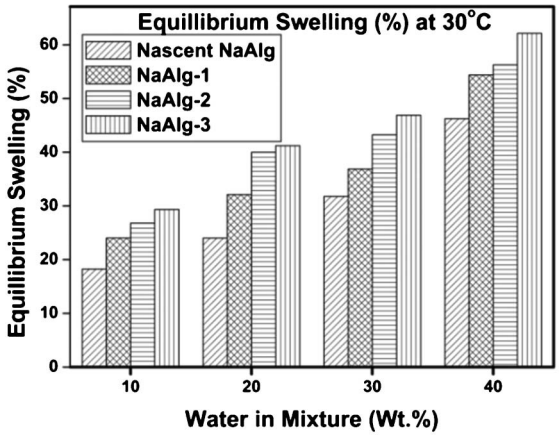

Fig. 6 Equilibrium swelling of membranes at different compositions of the water–IPA mixture at 30 °C, showing an increase in swelling with increase in FGS loading.

results for graphene oxide/polysulfone based mixed matrix membranes.

Sorption studies

Equilibrium swelling studies. In a PV process, liquid sorption through the nanocomposite membranes controls the transport of permeating molecules under the chemical potential gradient.[42] The results of % equilibrium swelling of nascent NaAlg and NaAlg nanocomposite membranes measured in water–IPA mixtures of various compositions presented in Fig. 6 show that as the % loading of FGSs increases, the % equilibrium swelling also increases, due to the polar nature of the FGSs. Also, a systematic increase of equilibrium swelling (%) can be seen with increasing concentration of feed water due to the water-selective nature of the nanocomposite membranes. At increasing concentrations of water in the feed mixture, an increase in the total permeance, but a decrease in selectivity is observed. This could be due to the plasticization effect of the membrane polymer in the presence of water, resulting in the swelling of the membrane, leading to a non-selective permeation.

Thermodynamic interactions. In pervaporation, solubility is a thermodynamic property, while diffusivity is a kinetic parameter and both of these would affect the membrane performance. In the solubility part, a change in concentration of one of the components, due to the presence of the other component, is caused by the interaction of the individual solvent components with the membrane polymer.[43] In the present study, the interaction parameters were estimated on the basis of swelling data using the well known Flory–Huggins theory:[44]

$$\ln \alpha_i = \ln \phi_i + (1 - \phi_i) + \chi_{ip}(1 - \phi_i)^2 \quad (7)$$

where α_i is the activity of the solvent, ϕ_i is the volume fraction, subscript i represents water or IPA and χ_{ip} is the Flory–Huggins interaction parameter between the polymer and the solvent. The volume fraction was computed using the equilibrium swelling data obtained in pure solvent media:

$$\phi_i = \frac{W_i \rho_i}{W_i/\rho_i + 1/\rho_m} \quad (8)$$

In the above equation, W_i is the solvent uptake (in terms of g g^{-1} of dry membrane) of component i at equilibrium; ρ_i and ρ_m are densities of the solvent and the membrane, respectively.

The density of the polymer (ρ_m) was measured by the benzene-displacement method by taking a known volume of benzene in a measuring cylinder. To this, a known weight of polymer was introduced and the volume of benzene displaced was measured, which was used to calculate the polymer density as:

$$\rho_m = \frac{W_m}{V_b} \quad (9)$$

where ρ_m is the density of the membrane, W_m is the weight of the membrane under consideration and V_b is the volume of benzene displaced. Using the values of ϕ_i, the membrane–polymer interaction parameter (χ_{ip}) was calculated as:[45]

$$\chi_{ip} = -\left(\frac{\ln \phi_i + (1-\phi_i)}{(1-\phi_i)^2}\right) \quad (10)$$

where χ_{ip} represents the chemical compatibility between the solvent i (either water or IPA) and the membrane polymer, p.

The polymer solubility parameter (δ) is a thermodynamic quantity that is closely related to the Flory–Huggins type interaction parameter χ_{ip}, which can be calculated using the equilibrium swelling data:[46]

$$\chi_{ip} = 0.35 + \frac{V_i}{RT}(\delta_i - \delta_p)^2 \quad (11)$$

Here, V_i is the molar volume of the solvent, R is the universal gas constant (8.314 J K^{-1} mol^{-1}) and T is the absolute temperature in Kelvin; δ_i and δ_p are the solubility parameters of the solvent and the membrane polymers, respectively. Taking the values of δ for water and IPA, respectively as 47.8 $J^{1/2}$ $cm^{-3/2}$ and 23.6 $J^{1/2}$ $cm^{-3/2}$, the δ_p of the polymer can be calculated from the following equation[46] derived from eqn (11):

$$\delta_p = \delta_i \pm \left[\frac{(\chi_{ip} - 0.35)RT}{V_i}\right]^{1/2} \quad (12)$$

Since eqn (12) has two roots, δ_p would theoretically assume either of the two values in determining the membrane–solvent solubility. When sorption is measured in two different solvents, one can select the one which matches best for the determination (in eqn (12), i = water).

In general, the lower the value of the Flory–Huggins interaction parameter, the greater the interaction.[47] The results of thermodynamic parameters for the membranes compiled in Table 1 suggest decreasing trends in χ_{1p} (water–

Table 1 Thermodynamic data on the membrane–permeate systems

Membranes	F–H interaction parameters		δ_p ($J^{1/2}$ $cm^{-3/2}$)	M_c (g mol^{-1})	$V_e \times 10^3$ (mol cm^{-3})
	χ_{1p}	χ_{2p}			
Nascent NaAlg	−15.208	−2.746	46.64	670	1.99
NaAlg-1	−24.084	−3.133	58.45	336	4.55
NaAlg-2	−27.292	−3.389	62.17	288	5.47
NaAlg-3	−31.765	−3.626	67.01	243	6.77

polymer interaction) and χ_{2p} (IPA–polymer interaction) values with increasing FGS concentration, which explains the observed increase in total permeance. The decrease in the χ_{1p} values is almost ten times higher than that of the χ_{2p} values, which suggests an increase in the water-selective nature of FGSs. Further, the values of δ_p increase continuously with increasing concentration of the FGSs, indicating an increase in the polar nature of the membrane. These observations are also supported by the water contact angle data discussed earlier.

Cross-link density. The results of the molar mass (M_c) between cross-links and cross-link density (V_e) were calculated using eqn (13) and (14), respectively:

$$\frac{1}{\overline{M_c}} = -\frac{\left(1/\rho_p V_i\right)\left[\ln(1-\phi_i)+\phi_i+\chi_{ip}{\phi_i}^2\right]}{{\phi_i}^{1/3}-(1/2)\phi_i} \quad (13)$$

$$V_e = \frac{\rho_m}{M_c} \quad (14)$$

In general, an increase in cross-linker concentration results in a decrease of M_c, thus giving an increase in V_e values.[48] The results presented in Table 1 show that the packing density increases with increasing FGS concentration. This would create more strained free pathways in the interstitial regions of the polymer matrix to facilitate the transport of liquid molecules. Notably, the results of M_c decrease systematically with increasing concentrations of the FGSs, suggesting a tighter polymer matrix at higher loadings of the FGSs.

Pervaporation performance

Effect of FGS concentration. All the membranes were found to be reusable for almost three times, with each membrane showing the best results for 10 h of continuous operation (with a 3% decrease in selectivity). As the FGS concentration increased, total permeance increased, which is consistent with the equilibrium swelling data. The contact angle results suggest an increase in hydrophilicity with increasing loading of the FGSs and hence, incorporation of the FGSs into NaAlg has a significant effect on both the permeance and the selectivity results as shown in Fig. 7 and the data presented in Table 2. Membrane performance was enhanced for FGS loading up to 2 wt.%, but above this concentration, membrane selectivity declines. This is attributed to self agglomeration of the FGS particles <2 wt.% (saturation limit) loading which results in a decrease in availability of the exposed surface for interaction with NaAlg. A similar trend was observed by He *et al.*,[49] for NaAlg–GO composites at 4 wt.% of GO loading for tensile strength studies. However, the PV studies being a more sensitive technique show a saturation limit at an even lower concentration.

The overall increase in the PV performance of the membranes after incorporating the FGSs may be due to the intercalation of the FGS layers within the intercalation spacing of 0.339 nm causing a higher resistance to the transport of bulky IPA molecules, which have a kinetic diameter of 0.47 nm compared to the value of 0.28 nm for water. Additionally, the water favourable intercalation formed between the FGSs and NaAlg restricts the permeation of IPA molecules (see Fig. 8). However, the presence of polar groups such as OH, COOH, carbonyl and ester on the surface of the FGSs might enhance the selective permeation of the polar water molecules rather than the less polar IPA. As the concentration of the FGSs increases in the membrane matrix, its performance increases, but at a concentration limit of 2 wt.%, the membrane exhibits superior performance and any further subsequent increase in FGS loading does not show an improved performance (*e.g.*, >3 wt.% loading). The performance of all the nanocomposite membranes is superior to that of the nascent NaAlg membrane. The interaction between the FGSs and NaAlg is shown in Fig. 8.

Effect of feed water composition. Table 2, as well as Fig. 9(a) and 9(b), display the effect of feed water composition, ranging from 10 to 40 wt.%, on the permeance and selectivity of the membranes. An increase in permeance at the cost of selectivity is observed. For NaAlg-2, an increase in feed water composition from 10 to 40 wt.% induced an increase in total

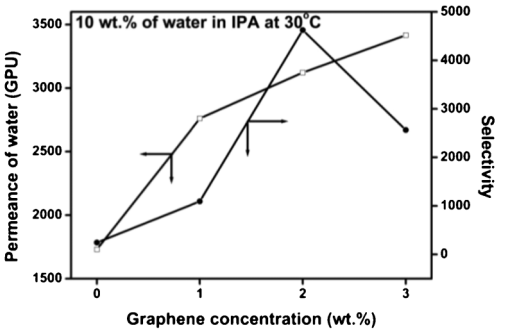

Fig. 7 Effect of filler loading on permeance and selectivity for nascent and FGS loaded NaAlg membranes at 30 °C.

Table 2 Relevant data on membrane performance at 30 °C

Membrane type	Feed water composition (wt. %)	E.S. (%)	J_w[a] (GPU)	J_e[a] (GPU)	Total permeance[a] (GPU)	α_{ij}	$K_w \times 10^6$ (m^3 (STP)/m^3 mmHg)	$K_{IPA} \times 10^8$ (m^3 (STP)/m^3 m^{-3} mmHg)	$D_w \times 10^8$ (m^2 s^{-1})	$D_{IPA} \times 10^{10}$ (m^2 s^{-1})
Nascent NaAlg	10	9	1730	7.07	1737	244	77	25	16.4	24.7
	20	15	3070	18.90	3089	162	100	48	25.7	38.5
	30	22	3698	29.08	3727	127	126	78	28.5	42.8
	40	38	4990	47.98	5038	104	187	140	31.2	46.8
NaAlg-1	10	13	2760	2.52	2763	1093	110	7	17.7	26.3
	20	19	3751	6.34	3757	591	138	18	21.2	32.2
	30	27	4070	13.06	4083	311	174	44	21.5	33.2
	40	44	6098	29.04	6127	210	251	94	28.1	39.1
NaAlg-2	10	14	3121	0.67	3122	4623	130	2	16.9	18.5
	20	20	3997	5.33	4002	749	158	16	19.6	25.3
	30	28	4338	11.98	4350	362	200	43	19.9	24.2
	40	45	7052	27.86	7080	253	275	85	27.2	36.9
NaAlg-3	10	15	3415	1.33	3416	2564	145	4	16.5	31.1
	20	21	4202	6.26	4208	671	175	20	18.2	33.5
	30	30	4704	13.96	4718	337	234	54	18.9	42.6
	40	48	7575	31.34	7606	241	312	101	25.8	45.2

[a] GPU = gas permeation unit = 10^{-6} cc (STP) cm^{-2} s^{-1} $cmHg^{-1}$.

permeance from 3122 to 7080 GPU, but selectivity decreased considerably from 4623 to 253. Equilibrium swelling studies also support these observations. This can be attributed to the presence of polar functional groups on NaAlg as well as the FGSs. As the water content in the feed mixture increases, more water molecules accumulate inside the polymer matrix, which increases the polymer segmental movement, such that the available fractional free-volume gets enlarged, leading to an increase in permeance. This adversely affects the membrane selectivity, a trade-off phenomenon that is typically observed in PV studies.[50] It can be observed that membranes with higher FGS concentrations are less vulnerable to an increase in feed water content.

Effect on sorption and diffusion coefficients. The transport of the binary liquid mixtures through PV membranes can be conventionally explained by a solution–diffusion mechanism, which occurs in three steps *viz.*, sorption, diffusion and evaporation. Evaporation is relatively faster, such that diffusion and sorption control the membrane performance.[51,52] The values of the diffusion co-efficient (D_i) were calculated using the equation:[33]

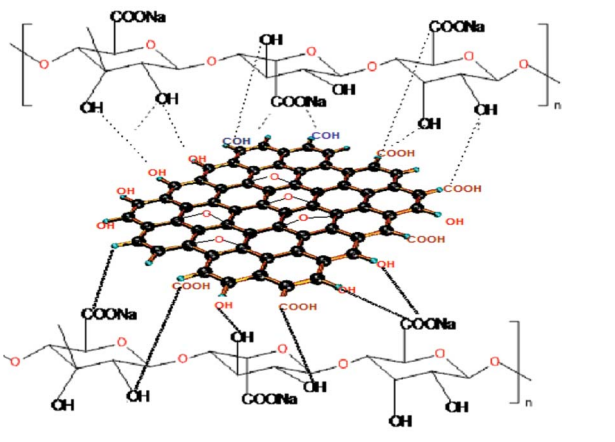

Fig. 8 Interaction between the FGSs and NaAlg.

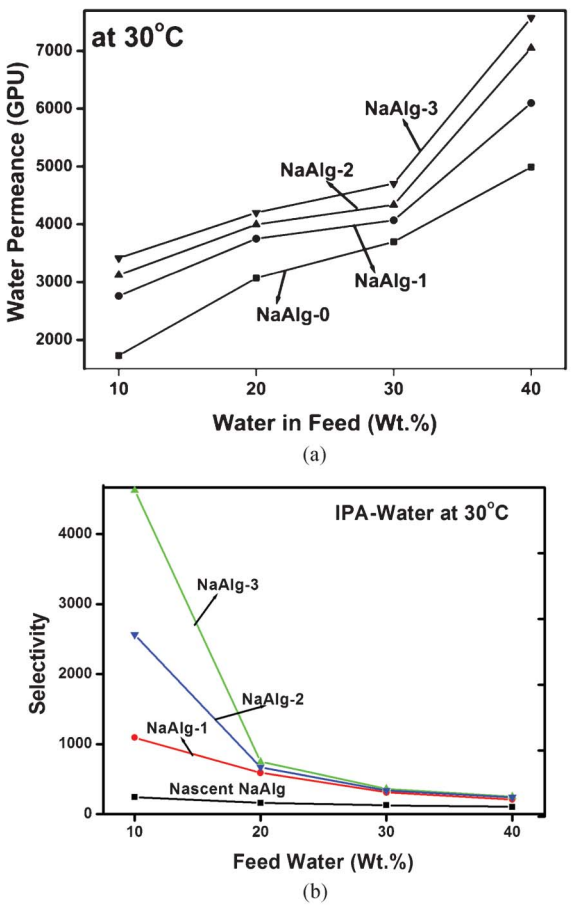

Fig. 9 (a) The concentration dependence of water permeance (GPU) through nascent and FGS loaded NaAlg at 30 °C. (b) The concentration dependence of selectivity of the nascent and FGS loaded NaAlg at 30 °C.

$$D_i = \frac{P_i}{K_i} \quad (15)$$

where P_i is the permeation flux per unit area (kg m^{-2} s^{-1}), D_i is the diffusion coefficient (m^2 s^{-1}), K_i is the sorption coefficient of the component i inside the membrane (m^3 (STP) m^{-3} $mmHg^{-1}$), subscript i stands for water or IPA. The sorption coefficient (K_i) is calculated as:

$$K_i = \frac{C_i}{p_i} \quad (16)$$

where C_i is the concentration (inside the membrane) and p_i is the partial pressure of the component i.

The calculated values of the sorption and diffusion coefficients of water and IPA at different feed water concentrations (10 to 40 wt.%) listed in Table 2 suggest higher values for water than IPA by at least two orders of magnitude, due to the water selective nature of the nanocomposite membranes. With increasing feed water concentration, sorption and diffusion coefficients of both water and IPA increased; as a result of this permeance also increased at the cost of selectivity. However, NaAlg-2 shows the lowest sorption and diffusion coefficient values for IPA, which results in it having the highest selectivity. In addition, by increasing the temperature as per the Arrhenius principles, the diffusion coefficients of water along with IPA increased incrementally.

Effect of temperature. PV performance of the nanocomposite membranes along with the nascent NaAlg membrane were tested at 30, 40, 50 and 60 °C for 10 wt.% of the water containing feed mixture. (see data presented in Fig. 10 for NaAlg-2). The permeation rate increased with increasing temperature with a significant decrease in selectivity.[53] Permeance followed the Arrhenius trend from which activation energy values for permeation and diffusion were calculated:

$$X = X_o \exp\left(\frac{-E_x}{RT}\right) \quad (17)$$

where X represents permeance (P) or diffusion coefficient (D), X_o is a constant representing the pre-exponential factor of J_o or D_o, E_x is the activation energy for permeation or diffusion, R is the universal gas constant and T is temperature in degrees Kelvin.

From the Arrhenius plots of $\ln(P_w/l)$ and $\ln D_w$ *vs.* $1/T$ (not displayed to avoid overcrowding) and from the least squares fits of these linear plots, activation energy values of water permeance (E_{pw}) and diffusion (E_{Dw}) were calculated. In a similar manner, the activation energy of IPA permeance (E_{pIPA}) and diffusion (E_{DIPA}) were calculated (see Table 3). Generally, diffusion and permeation of molecules is inversely proportional to the Arrhenius activation energy values.[35] The results of E_{pi} (for both water and IPA) of the nanocomposite membranes are higher than that of the nascent NaAlg. All the membranes exhibit higher E_{pIPA} and E_{DIPA} values than E_{Dw} and E_{pw}, indicating the water selective nature of the membranes. Further, with an increase in FGS concentration, the E_{pw} values increases incrementally, but E_{pIPA} values increase by one order of magnitude, which shows the easier permeation of water molecules due to the polymer modification. On the other hand, the E_{Di} values decrease with an increase in E_{DIPA} values as the graphene concentration increased, which confirms the water selective diffusion pathway in the interstitial regions of the matrix. The E_{pIPA} and E_{DIPA} values obtained for NaAlg-2 are higher than the other membranes, which explain its superior water selective nature.

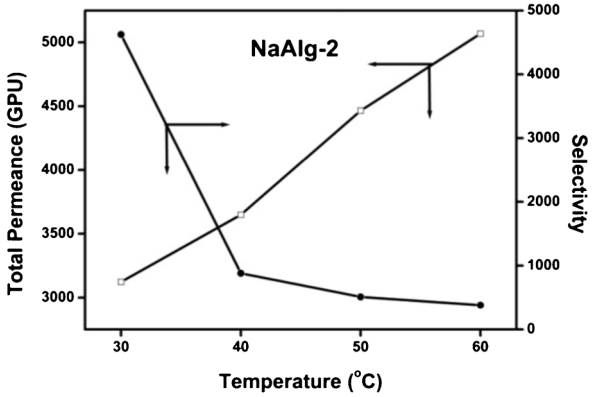

Fig. 10 The temperature dependence of permeance (GPU) and selectivity for NaAlg-2 for feed concentration of 10 wt.% of water in IPA.

The heat of sorption values were calculated from the energy of activation data as:

$$\Delta H_s = E_{pi} - E_{Di} \quad (18)$$

The ΔH_s values included in Table 3 give information about the nature of transport phenomena, which involves the combined effect of Henry's and Langmuir's type sorption.[54] Henry's law implies that the heat of sorption follows an endothermic process for liquid transport, thus leading to the dissolution of the chemical species into the site within the membrane. On the other hand, Langmuir's sorption requires the pre-existence of a site in which sorption occurs only by the hole-filling mechanism, which gives rise to an exothermic contribution. The ΔH_s values obtained in this study are negative (exothermic contribution) for all the membranes, indicating that Langmuir's type sorption is predominant.

Comparison of present data with the literature. A number of studies have been reported in the literature[55–61] concerning the PV dehydration of an IPA–water mixture. Table 4 displays

Table 3 Arrhenius activation parameters of different systems in kJ mol^{-1}

Membranes	E_{pw}[a]	E_{Dw}[c]	ΔH_s[e]	E_{pIPA}[b]	E_{DIPA}[d]	ΔH_s[e]
Nascent NaAlg	9.63	33.24	−23.61	30.63	69.06	−38.43
NaAlg-1	15.00	23.37	−8.37	53.63	78.88	−25.25
NaAlg-2	14.04	22.55	−8.51	105.76	109.34	−3.58
NaAlg-3	13.51	20.56	−7.05	83.79	89.11	−5.32

[a] E_{pw} – activation energy for water permeance. [b] E_{pIPA} – activation energy of IPA permeance. [c] E_{Dw} – activation energy for diffusion of water. [d] E_{DIPA} – activation energy for diffusion of IPA. [e] ΔH_s – difference in activation energies of permeance and diffusion.

Table 4 Comparison of water permeability and selectivity of the present membranes with literature data

Membrane type	Feed water (wt.%)	Temperature (°C)	Water Permeability (Barrer)	Selectivity	Ref.
PAI-polyamide TFC[a]	15	50	2720	1019	[55]
F2PVGLU6	12.265	40	106 100	97	[56]
GOTMS incorporated polyamide membranes	15	50	3669	453	[57]
Tarlon/P84 blended hollow fiber	15	60	80 180	314	[58]
6 FDA-ODA-NDA/Ultem hollow fiber	15	60	100 530	5781	[59]
PEC^{+}/PEC^{-} layer by layer film	10	50	8601	1043	[60]
NaCMC/PVA and 20 wt.% of 13X zeolite.	10	35	103 480	5138	[61]
NaAlg and 2 wt.% FGSs	10	30	156 100	4623	Present work

[a] PAI – polyamide; TFC – thin film composite; F2PVGLU – 2 wt.% of glutaraldehyde in polyvinyl alcohol and 6 wt.% of glutaraldehyde; 3-glycidyloxypropyltrimethoxy-silane (GOTMS); sodium carboxymethylcellulose (NaCMC) (1 Barrer = 1×10^{-10} cm^3 (STP) cm cm^{-2} s^{-1} $cmHg^{-1}$).

the membrane performance data with those reported in terms of driving force normalized permeability and selectivity. Permeability in Barrer and selectivity data of various reported membranes were recalculated from their available flux and separation factor data using eqn (2) and [(6) times the thickness of the membrane]. It is observed that some published data show high permeability with low selectivity such as the permeability of 106 100 Barrer and selectivity of 453 as observed in the case of the thin film composite of 2 wt.% of gluteraldehyde in poly(vinyl alcohol).[56] While the other literature data show high selectivity at high concentrations of filler *viz.*, selectivity of 5138 and good permeability of 103 480 Barrer as observed for 20 wt.% 13X zeolite-loaded sodium carboxymethyl cellulose and poly(vinyl alcohol) blends.[61] The membranes of this study show both high permeability and good selectivity as we were able to achieve such a performance at lower concentration (2 wt.%) of the FGSs.

Conclusions

FGS-loaded NaAlg membranes were fabricated and tested for PV dehydration of IPA at varying feed concentrations and temperatures. The membranes display a reasonably high degree of permeance and selectivity. XRD data show a decrease in crystalline domains with an increase in FGS loading, which suggest the progressive improvement in confinement of the polymer chains by the filler particles. FTIR spectra showed an enhancement in hydrogen bonding between polymer and filler with increasing FGS concentration. Contact angle data proved the membrane hydrophilicity enhancement due to the presence of the FGSs, whereas thermal stability enhancement was indicated by TGA. Uniform dispersion of the FGS particles in the NaAlg matrix was demonstrated by FE-SEM images. Owing to the high surface area and polar functionalization of the FGSs, a water selective interface is likely to be formed within the NaAlg matrix. However, at FGS concentrations up to <2 wt.%, both selectivity and permeance increased, but at higher concentrations, selectivity was lost due to an increase in particle agglomeration. Thermodynamic and kinetic parameters demonstrated a four-fold increase in water selectivity. Arrhenius energy parameters demonstrated an IPA energy barrier one order of magnitude higher compared to that of water. The experimentally determined packing density parameter confirms an increase in packing density with an increase in the FGS concentration. Further improvement in membrane performance can be expected by improving the dispersion of the FGSs in the membrane matrix. Any effort in this direction would yield still improved results.

Acknowledgements

Financial assistance from the Vision Group of Science and Technology (VGST), Government of Karnataka and Admar Mutt Education Foundation, Bangalore are gratefully acknowledged. DPS is thankful to Manipal University for permitting this research as a part of the Ph.D. programme. The authors thank Prof. Hans Wijmans (Membrane Technology and Research, CA, USA) for his kind help to recast the present data in the form of driving force normalized permeance and real selectivity.

References

1 V. V. Hoof, L. V. Abeele, A. Buekenhoudt, C. Dotremont and R. Leysen, *Sep. Purif. Technol.*, 2004, **37**, 33–49.
2 S. Widagdo and W. D. Seider, *AIChE J.*, 1996, **42**, 96–130.
3 F. Lipnizki, R. W. Field and P. K. Ten, *J. Membr. Sci.*, 1999, **153**, 183–210.
4 X. Feng and R. Y. M. Huang, *Ind. Eng. Chem. Res.*, 1997, **36**, 1048–1066.
5 A. M. Urtiaga, E. D. Gorri and I. Ortiz, *Sep. Purif. Technol.*, 2006, **49**, 245–252.
6 S. L. Wee, C. T. Tye and S. Bhatia, *Sep. Purif. Technol.*, 2008, **63**, 500–516.
7 R. W. V. Gemert and F. P. Cuperus, *J. Membr. Sci.*, 1995, **105**, 287–291.
8 P. Shao and R. Y. M. Huang, *J. Membr. Sci.*, 2007, **287**, 162–179.
9 S. D. Bhat and T. M. Aminabhavi, *Sep. Purif. Rev.*, 2007, **36**, 203–229.

10 S. D. Bhat and T. M. Aminabhavi, *Microporous Mesoporous Mater.*, 2006, **91**, 206–214.
11 S. D. Bhat and T. M. Aminabhavi, *Sep. Purif. Technol.*, 2006, **51**, 85–94.
12 D. A. Devi, B. Smitha, S. Sridhar and T. M. Aminabhavi, *J. Membr. Sci.*, 2005, **262**, 91–99.
13 V. T. Magalad, G. S. Gokavi, M. N. Nadagouda and T. M. Aminabhavi, *J. Phys. Chem. C*, 2011, **115**, 14731–14744.
14 V. T. Magalad, G. S. Gokavi, C. Ranganathaiah, M. H. Burshe, C. Han, D. D. Dionysiou, M. N. Nadagouda and T. M. Aminabhavi, *J. Membr. Sci.*, 2013, **430**, 321–329.
15 V. T. Magalad, A. R. Supale, S. P. Maradur, G. S. Gokavi and T. M. Aminabhavi, *Chem. Eng. J.*, 2010, **159**, 75–83.
16 S. G. Adoor, B. Prathab, L. S. Manjeshwar and T. M. Aminabhavi, *Polymer*, 2007, **48**, 5417–5430.
17 R. Mahajan, R. Burns, M. Schaeffer and W. J. Koros, *J. Appl. Polym. Sci.*, 2002, **86**, 881–890.
18 S. G. Adoor, M. Sairam, L. S. Manjeshwar, K. V. S. N. Raju and T. M. Aminabhavi, *J. Membr. Sci.*, 2006, **285**, 182–195.
19 X. Huang, X. Qi, F. Boey and H. Zhang, *Chem. Soc. Rev.*, 2012, **41**, 666–686.
20 M. J. Allen, V. C. Tung and R. B. Kaner, *Chem. Rev.*, 2010, **110**, 132–145.
21 T. Kuila, S. Bose, A. K. Mishra, P. Khanra, N. H. Kim and J. H. Lee, *Prog. Mater. Sci.*, 2012, **57**, 1061–1105.
22 T. Kuilla, S. Bhadra, D. Yao, N. H. Kim, S. Bose and J. H. Lee, *Prog. Polym. Sci.*, 2010, **35**, 1350–1375.
23 H. Kim and C. W. Macosko, *Polymer*, 2009, **50**, 3797–3809.
24 R. R. Nair, H. A. Wu, P. N. Jayaram, I. V. Grigorieva and A. K. Geim, *Science*, 2012, **335**, 442–444.
25 J. T. Choi, T. D. Dao, K. M. Oh, H. Li, H. M. Jeong and B. K. Kim, *Smart Mater. Struct.*, 2012, **21**, 75017–75025.
26 M. J. McAllister, J.-L. Li, D. H. Adamson, H. C. Schniepp, A. A. Abdala, J. Liu, M. Herrera-Alonso, D. L. Milius, R. Car, R. K. Prud'homme and I. A. Aksay, *Chem. Mater.*, 2007, **19**, 4396–4404.
27 F. U. Nigiz, H. Dogan and N. D. Hilmioglu, *Desalination*, 2012, **300**, 24–31.
28 T. M. Aminabhavi and H. G. Naik, *J. Appl. Polym. Sci.*, 2002, **83**, 244–258.
29 J. G. Wijmans, *J. Membr. Sci.*, 2003, **220**, 1–3.
30 Gmehling, Onken and Arlt, *DECHEMA Chemistry Data Series*, Vol. 1, part 1b, 1977.
31 W. F. Guo, T. S. Chung, T. Matsuura, R. Wang and Y. Liu, *J. Appl. Polym. Sci.*, 2004, **91**, 4082–4060.
32 M. J. Holmes and M. V. Winkle, *Ind. Eng. Chem.*, 1970, **62**, 21–31.
33 R. W. Baker, J. G. Wijmans and Y. Huang, *J. Membr. Sci.*, 2010, **348**, 346–352.
34 G. X. Wang, B. Wang, J. S. Park, J. Yang, X. P. Shen and J. Yao, *Carbon*, 2009, **47**, 68–72.
35 V. T. Magalad, G. S. Gokavi, K. V. S. N. Raju and T. M. Aminabhavi, *J. Membr. Sci.*, 2010, **354**, 150–161.
36 S. H. Choi, D. H. Kim, A. V. Raghu, K. R. Reddy, H.-I. Lee, K. S. Yoon, H. M. Jeong and B. K. Kim, *J. Macromol. Sci., Part B: Phys.*, 2012, **51**, 197–207.
37 S. Hua, H. Ma, X. Li, H. Yang and A. Wang, *Int. J. Biol. Macromol.*, 2010, **46**, 517–523.
38 L. H. Tang, Y. Wang, Y. M. Li, H. B. Feng, J. Lu and J. H. Li, *Adv. Funct. Mater.*, 2009, **19**, 2782–2789.
39 D. Han, L. Yan, W. Chen and W. Li, *Carbohydr. Polym.*, 2011, **83**, 653–658.
40 N. A. Travlou, G. Z. Kyzas, N. K. Lazaridis and E. A. Deliyanni, *Chem. Eng. J.*, 2013, **217**, 256–265.
41 B. M. Ganesh, A. M. Isloor and A. F. Ismail, *Desalination*, 2013, **313**, 199–207.
42 T. M. Aminabhavi, R. S. Khinnavar, S. B. Harogoppad, U. S. Aithal, Q. T. Nguyen and K. C. Hansen, *J. Macromol. Sci., Part C*, 1994, **34**, 139–204.
43 M. H. V. Mulder, T. Franken and C. Smolders, *J. Membr. Sci.*, 1985, **22**, 155–173.
44 P. J. Flory, *Principles of Polymer Chemistry*, Cornell University Press, Ithaca, NY, 1953.
45 G. M. Bristow and W. F. Watson, *Trans. Faraday Soc.*, 1958, **54**, 1731–1741.
46 J. Brandrup, E. H. Immergut and E. A. Grulke, *Polymer Hand Book*, Wiley/Interscience, New York, 1999.
47 Q. G. Zhang, Q. L. Liu, Z. Y. Jiang, L. Y. Ye and X. H. Zhang, *Microporous Mesoporous Mater.*, 2008, **110**, 379–391.
48 H. Lin, T. Kai, B. D. Freeman, S. Kalakkunnath and D. S. Kalika, *Macromolecules*, 2005, **38**, 8381–8393.
49 Y. He, N. Zhang, Q. Gong, H. Qiu, W. Wang, Y. Liu and J. Gao, *Carbohydr. Polym.*, 2012, **88**, 1100–1108.
50 M. B. Patil, R. S. Veerapur, S. A. Patil, C. D. Madhusoodana and T. M. Aminabhavi, *Sep. Purif. Technol.*, 2007, **54**, 34–43.
51 J. G. Wijmans and R. W. Baker, *J. Membr. Sci.*, 1995, **107**, 1–21.
52 A. Yamasaki, T. Iwatsubo, T. Masuoka and K. Mizoguchi, *J. Membr. Sci.*, 1994, **89**, 111–117.
53 R. Y. M. Huang and C. K. Yeom, *J. Membr. Sci.*, 1991, **58**, 33–47.
54 D. H. Weinkauf and D. R. Paul, *ACS Symposium series*, Washington, DC, 1990, vol. 423, pp. 61–91.
55 J. Zuo, Y. Wang, S. P. Sun and T. S. Chung, *J. Membr. Sci.*, 2012, **405–406**, 123–133.
56 P. Das, S. K. Ray, S. B. Kuila, H. S. Samanta and N. R. Singha, *Sep. Purif. Technol.*, 2011, **81**, 159–173.
57 J. Zuo, Y. Wang and T. S. Chung, *J. Membr. Sci.*, 2013, **433**, 60–71.
58 M. M. Teoh, T. S. Chung, K. Y. Wang and M. D. Guiver, *Sep. Purif. Technol.*, 2008, **61**, 404–413.
59 N. Widjojo and T. S. Chung, *Chem. Eng. J.*, 2009, **155**, 736–743.
60 Q. Zhao, J. Qiao, Q. An and Z. Sun, *J. Membr. Sci.*, 2010, **346**, 335–343.
61 C. V. Prasad, B. Yeriswamy, H. Sudhakar, P. Sudhakara, M. C. S. Subha and J. I. K. C. Rao, *J. Appl. Polym. Sci.*, 2012, **125**, 3351–3360.

